ACS OMEGA

Article

Cite This: ACS Omega 2018, 3, 18275−18284

http://pubs.acs.org/journal/acsodf

Application of Industrial Wastes from Chemically Treated Aluminum Saline Slags as Adsorbents

Antonio Gil,*[,†] Ekhine Arrieta,[†] Miguel Ángel Vicente,[‡] and Sophia A. Korili[†]

[†]INAMAT-Departamento de Ciencias, Edificio de los Acebos, Universidad Pública de Navarra, Campus de Arrosadía, E-31006 Pamplona, Spain

[‡]GIR-QUESCAT, Departamento de Química Inorgánica, Universidad de Salamanca, E-37008 Salamanca, Spain

Supporting Information

ABSTRACT: In this study, industrial wastes, which remain after aluminum extraction from saline slags, were used as adsorbents. The aluminum saline slags were treated under reflux with 2 mol/dm^3 aqueous solutions of NaOH, H_2SO_4, and HCl for 2 h. After separation by filtration, aqueous solutions containing the extracted aluminum and residual wastes were obtained. The wastes were characterized by nitrogen adsorption at −196 °C, X-ray diffraction, scanning electron microscopy, and ammonia pulse chemisorption. The chemical treatment reduced the specific surface area, from 84 to 23 m^2/g, and the pore volume, from 0.136 to 0.052 cm^3/g, of the saline slag and increased the ammonia-adsorption capacity from 2.84 to 5.22 cm^3/g, in the case of acid-treated solids. The materials were applied for the removal of Acid Orange 7 and Acid Blue 80 from aqueous solutions, considering both single and binary systems. The results showed interesting differences in the adsorption capacity between the samples. The saline slag treated with HCl rapidly adsorbed all of the dyes present in solution, whereas the other materials retained between 50 and 70% of the molecules present in solution. The amount of Acid Orange 7 removed by the nontreated material and by the material treated with NaOH increased in the presence of Acid Blue 80, which can be considered as a synergistic behavior. The CO_2 adsorption of the solids at several temperatures up to 200 °C was also evaluated under dry conditions. The aluminum saline slag presented an adsorption capacity higher than the rest of treated samples, a behavior that can be explained by the specific sites of adsorption and the textural properties of the solids. The isosteric heats of CO_2 adsorption, determined from the Clausius−Clapeyron equation, varied between 1.7 and 26.8 kJ/mol. The wastes should be used as adsorbents for the selective removal of organic contaminants in wastewater treatment.

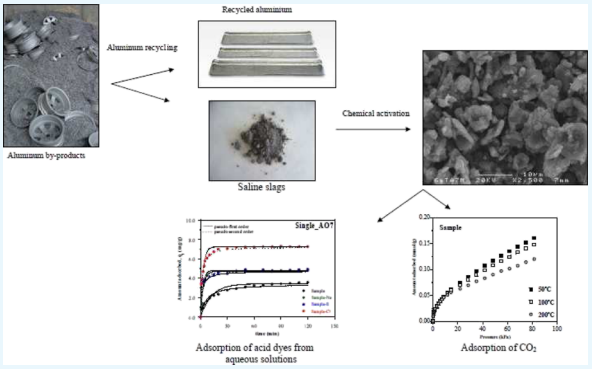

1. INTRODUCTION

Related to their complex aromatic structures, dyes present in industrial effluents create bad taste, odors, and unsightly color and can even have carcinogenic effects even at low concentrations. Acid dyes are more problematic than basic ones because anions are very weakly retained by most soil components and hence cause contamination of surface waters.[1] Adsorption technologies have been proven to be effective and cost-efficient for treating wastewaters with the presence of organic contaminants because of their design simplicity, insensitivity to toxic substances, and high efficiency.[2,3] Several adsorbents, including activated carbons and zeolites, among others, are commonly used for this purpose. In addition, development of low-cost adsorbents from industrial wastes has a growing interest; among them, activated saline slags generated during secondary aluminum melting processes are considered to be interesting materials for being used in this field, as previously reported by our research groups.[4]

Multiple organic contaminants are usually found in wastewater systems, suggesting possible interactions between these organic molecules. The competitive effects between these coexisting simultaneous contaminants on removal must therefore be considered to study how these molecules can be removed from wastewater. Although several studies have reported adsorption processes for single-component systems,[3] limited studies have considered the adsorption of organic molecules in multiple systems.[5−25] For example, the adsorption of three acid dyes, namely Acid Blue 80, Acid Red 114, and Acid Yellow 117, on an activated carbon showed that the molecular size and chemical groups can contribute to the relative differences found for the adsorption capacities of these three dyes.[6] Similarly, the activated carbon produced from the phosphoric acid treatment of waste bamboo scaffolding and activated at several temperatures was evaluated as an adsorbent for two acid dyes by Chan et al.,[15] who reported an effect of the porosity of the activated carbons and the molecular size of

Received: September 15, 2018
Accepted: December 12, 2018
Published: December 26, 2018

DOI: 10.1021/acsomega.8b02397
ACS Omega 2018, 3, 18275−18284

the dyes on the adsorption capacity. In a related study, the simultaneous removal of two industrial dyes by adsorption and photocatalysis on a fly ash TiO_2 composite was studied by Duta and Visa,[20] and they found that the efficiency of adsorption strongly depended on the microporous structure of the adsorbent and that the kinetics depended on the flexibility of the dyes. A mixed biosorbent containing carboxyl and amine groups was prepared by Yu et al.[21] to treat an aqueous solution containing cationic and anionic dyes, namely Basic Red 9 and Direct Red 28, whereas Yang et al.[23] reported $MnFe_2O_4$ as an adsorbent for the removal of Basic Blue 9 and Direct Red 28 in single and binary systems. Considering single solutions, the adsorption rate for Basic Blue 9 was generally higher than that for Direct Red 28, and the adsorption equilibrium time for Basic Blue 9 was shorter than that for Direct Red 28. The interaction between the dyes showed a synergistic effect, where the adsorption of Direct Red 28 on the adsorbent was promoted. The surface and porosity properties of the adsorbents and the characteristics of the adsorbates are, in general, the factors that most affect the adsorption process.

CO_2 emissions to the atmosphere must be controlled to reduce the CO_2 levels that affect global warming. Adsorbents such as zeolites, carbon-derived materials, hydrotalcites, amine-functionalized mesoporous silicas, and metal organic frameworks have been considered as potential solids to capture CO_2.[26−30] The CO_2 uptake capacities under several conditions of temperature and pressure, the stability in the presence of water, and the conditions for the regeneration of the materials have been evaluated as important aspects to select the suitable adsorbents. The development of effective low-cost and renewable CO_2 adsorbents is also mandatory. With these ideas, CO_2 adsorbents from waste precursors have been reported, including byproducts derived from coal, biomass, water treatment, eggshells and mussel shells, lime mud, and fly ash, among others.[31−34]

In the present study, industrial wastes resulting from the extraction of aluminum from saline slag wastes were selected as porous adsorbents for the uptake of Acid Blue 80 and Acid Orange 7 from aqueous solutions, including both single and binary systems, and of CO_2 in the temperature interval from 50 to 200 °C and pressures up to 80 kPa. As a first objective, the study included the assessing of the competitive behavior of Acid Orange 7 and Acid Blue 80 in single and binary solutions. As a second objective, the study considered the capacity of CO_2 adsorption of the adsorbents at three temperatures and up to a pressure of 80 kPa and the estimation of the isosteric heat of adsorption using the Clausius−Clapeyron equation.

2. RESULTS AND DISCUSSION

2.1. Characterization of the Adsorbents. Acid and alkaline material treatments have been widely studied for the elimination of mineral impurities, disaggregation of particles, and dissolution of elements such as Mg^{2+} or Al^{3+}. Depending on the intensity and the type of material, the treatment could produce modification of the textural properties and the number of acid centers.[4] When H_3PO_4 or H_2SO_4 is used in the treatment, the incorporation of PO_4^{3-} or SO_4^{2-} onto the surface of the materials can take place, which may affect their interaction with adsorbate molecules.

The N_2 adsorption−desorption results for samples at −196 °C are summarized in Figure 1. The adsorption isotherms are of type II in the BDDT classification,[35] with an H3-type hysteresis loop.[36] The hysteresis loop is related to materials

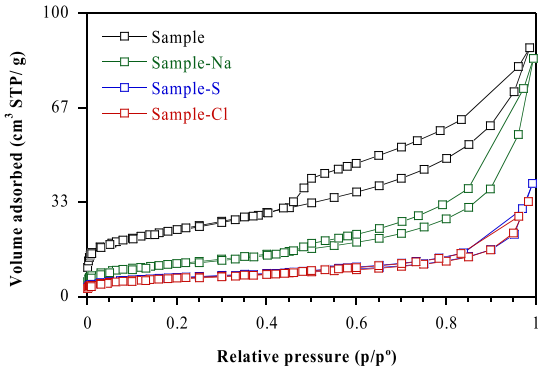

Figure 1. Experimental isotherms for the adsorption of nitrogen at −196 °C.

comprising aggregates of platelike particles forming slitlike pores. The nitrogen adsorption capacity decreases with the chemical treatment. In the case of *sample-S* and *sample-Cl*, both samples show almost the same capacity. The results related to the textural properties of the reference sample and the activated samples are listed in greater detail in Table 1. Treatment under reflux conditions with water did not have a marked effect on the textural properties of the reference sample. In contrast, the specific surface area and pore volume of the sample decreased when treated with acids or bases. The specific surface area decreases between 50 and 73% and the total volume of pores decreases between 4 and 62%. Average pore sizes increase with treatment, from 15.7 to 24.6 nm. These findings suggest that a porous solid is dissolved during the treatments, mainly under acid conditions. These results are in accordance with those obtained previously, where the effect of time and concentration of various chemical reagents was studied.[4]

The powder X-ray diffraction (XRD) pattern for *sample-Na* is very similar to that of *sample* (Figure 2), in agreement with the fact that the raw sample was previously treated with water at high temperature to remove the soluble salts usually present in this type of waste, and this washing was actually carried out under alkaline conditions as a consequence of the presence of nitrides in the raw sample.[37] In the case of the samples treated with acids, some diffraction peaks for the original sample, such as those for calcite, disappear, whereas others, such as those for calcium and magnesium sulfate, appear after the sample is treated with H_2SO_4. This suggests that Ca^{2+} is dissolved from the slag by the acid treatment, that is, from calcite and calcium aluminate, but it then precipitates as sulfate because of the insolubility of this salt. The chemical composition of this type of waste is very complex and depends on the raw material used. The main crystalline phases detected by various authors include aluminum oxide (various phases), metallic Al, magnesium aluminate, magnesium oxide, and calcium aluminate.[38−40] The main peaks from these phases are marked in Figure 2, confirming their presence in our slag. The presence of other compounds (or elements) was not detected although it cannot be ruled out; they may be in the form of amorphous phases or also as crystalline phases but in very low amounts, in both cases not detected by XRD.

The morphology changes caused by the chemical treatments are compared from the scanning electron microscopy (SEM) images for the four samples (Figure 3). No significant differences can be observed between *sample* (A) and *sample-Na* (B). The particles from *sample-S* (C) had a small size and

DOI: 10.1021/acsomega.8b02397
ACS Omega 2018, 3, 18275−18284

Table 1. Specific Surface Areas, Pore Volumes, Pore Diameters, pzc, and Acidity Properties of the Samples

	S_{BET} [a] (m^2/g)	S_{ext} [b] (m^2/g)	V_{pT} [c] (cm^3/g)	$V_{\mu p}$ [b] (cm^3/g)	d_{pBJH} (nm)	pHpzc	$V(NH_3)$ (cm^3/g)
sample	84	64	0.136	0.010	15.7	8.6	2.84
sample-Na	42	38	0.130	0.002	24.2	9.7	3.35
sample-S	24	14	0.062	0.005	24.6	2.0	5.21
sample-Cl	23	13	0.052	0.005	24.3	3.7	5.22

[a]Brunauer−Emmett−Teller (BET) specific surface area calculated in the relative pressure range of 0.05−0.20. [b]External surface area and micropore volume estimated from the *t*-plot method. [c]Total pore volume calculated at a relative pressure of 0.99.

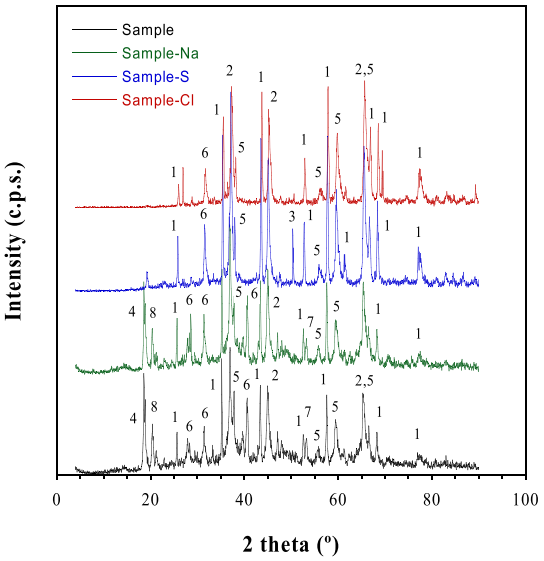

Figure 2. XRD patterns for the samples. [(1) Al_2O_3, ICDD 46-1212], [(2) metallic Al], [(3,8) $CaSO_4$, ICDD 36-0432], [(4) calcite, ICDD 05-0586], [(5) $MgAl_2O_4$, ICDD 21-1152], [(6) calcium aluminate, ICDD 70-0134], and [(7) MgO, ICDD 45-946].

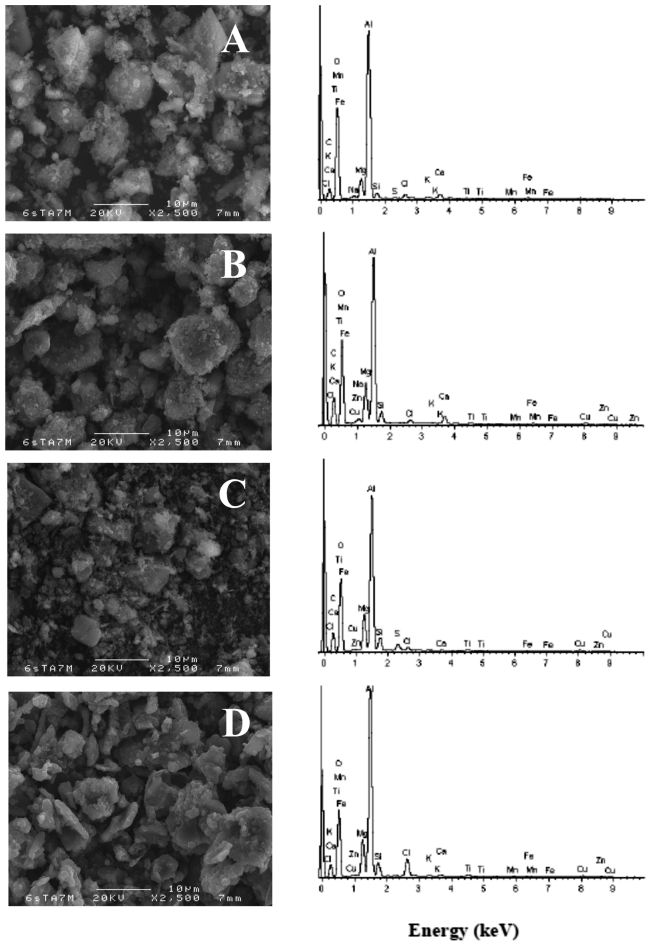

Figure 3. SEM images and EDX analysis for the samples. (A) Sample, (B) sample-Na, (C) sample-S, and (D) sample-Cl.

had the tendency to form aggregates. This characteristic was not showed for the sample treated with HCl, *sample-Cl* (D). The qualitative composition of the samples is also characterized by energy-dispersive X-ray (EDX) analysis. Several metals and metal oxides are detected indicating the complexity of the samples as an industrial waste. The presence of S in *sample-S* is also confirmed.

Ammonia chemisorption provides a measure of the concentration of acid sites. The total acidity results, as $cm_{NH_3}{}^3/g$, are given in Table 1. The acidity of the samples increases from 2.84 to 5.22 cm^3 NH_3/g after the activation treatment, mainly in the case of samples treated with acids.

2.2. Dye Adsorption Experiments. The contact time is a parameter that is known to control adsorption processes to determine the equilibrium time.

The pH conditions strongly influence the adsorption processes, as they condition the charge of the dye molecules, the charge of the solid surface, and so forth. Thus, to evaluate the effect of solution pH, 0.2 g of the *sample* was added to 100 cm^3 of aqueous solutions containing 15 mg/dm^3 of AB80 or AO7 (0.022 and 0.042 $mmol/dm^3$, respectively) at various pH values in the range of 2−9. The resulting suspensions were shaken for 120 min. The maximum percentage of dye removal was observed at pH 2, which is explained by the electrostatic interactions between the adsorbate and the surface of the adsorbents. One of the main parameters reported to govern adsorption is the point of zero charge (pzc) of the surface of the solids. By this reason, the pHpzc of solids, *sample*, *sample-Na*, *sample-Cl*, and *sample-S*, was determined according to the method previously reported[41] and found to be 8.6, 9.7, 3.7, and 2.0, respectively (see Table 1). Under the pH conditions for adsorption, all samples show a positively charged surface; therefore adsorption is improved at acidic pH. In the case of the dye molecules, the values of pK_a must be taken into account (see Table S1, Supporting Information). Similar trends have been reported by other authors, such as Kyzas et al.,[42] who described the adsorption of Acid Orange 7 and Acid Green 25 on the surface of cerium oxide. Also considering that a lot of industrial wastewater is strongly acidic, a pH value of 2 was selected for the additional experiments.

The evolution of the amounts of dye adsorbed with time for the single solutions is shown in Figure 4. Dye removal was rapid in the initial stages, reaching equilibrium after around 40 min. Moreover, AB80 adsorbs more rapidly than AO7. The factors affecting the adsorption selectivity of an adsorbent for

DOI: 10.1021/acsomega.8b02397
ACS Omega 2018, 3, 18275−18284

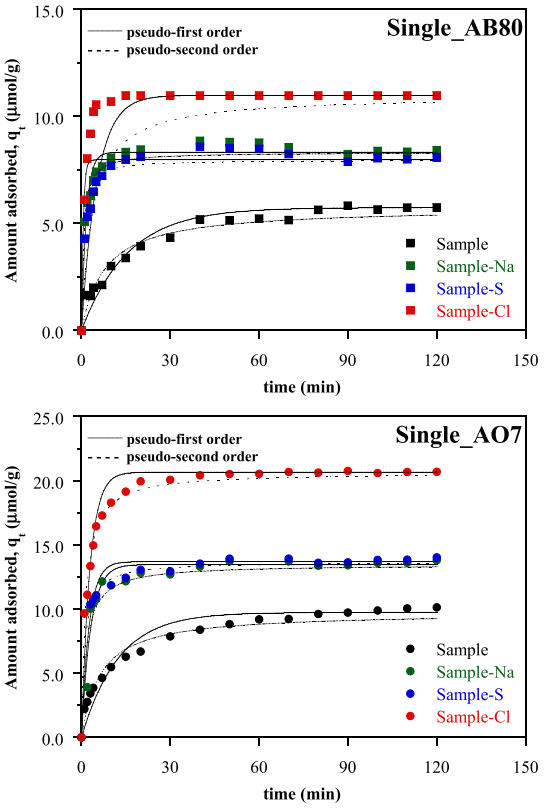

Figure 4. Kinetic adsorption data of AB80 and AO7 using samples as adsorbents. T = 25 °C, C_0 = 15 mg/dm^3 (0.022 mmol/dm^3 for AB80 and 0.022 mmol/dm^3 for AO7), and pH = 2. The lines represent a pseudo-first-order model (—) and a pseudo-second-order model (---).

several kinds of adsorbates may be related to the characteristics of the active sites (functional groups, porous structure, surface properties, etc.), the characteristics of the adsorbates (molecular structure, ionic nature, etc.), and the solution chemistry (ionic strength, pH, etc.).[4,6,10,11,13] The adsorption of acidic dyes is mostly governed by physical adsorption; therefore, the structure of these dyes could be the principal factor that affects the adsorption capacity.[8] The acidic dyes used in this study contain two (AB80) and one sulfonic acid groups (AO7) (see Table S1, Supporting Information), and therefore these differences could explain their adsorption behavior when only one adsorbate is considered. Several authors have explained the results found for other dyes on the basis of the structures of the molecules and the porosity properties of the adsorbents, mainly activated carbons, which have high specific surface areas.[15,20,42,43] In the case of industrial wastes, which do not tend to be carbon-based, the chemical surface properties should be taken into consideration when explaining the removal of dyes from aqueous solutions. In general, the adsorption capacity of the waste increased after chemical treatment with HCl, H_2SO_4, and NaOH (see the results summarized in Figure 4). Thus, the adsorption capacity of the activated wastes increased from 9.7 μmol/g for AO7 and the nonactivated waste (*sample*) to 20.7 μmol/g for the activated waste treated with HCl (*sample-Cl*). The wastes treated with NaOH and H_2SO_4 showed the same adsorption capacity, 13.6 μmol/g. In the case of AB80, the adsorption capacities obtained were 5.7 (*sample*), 8.0 (*sample-S*), 8.3 (*sample-Na*), and 11.0 μmol/g (*sample-Cl*). The efficiency of adsorption was also determined by taking into account the amounts of dyes adsorbed and the initial amounts brought into contact with the adsorbents. In general, the adsorbents removed more AB80 than AO7, probably because of the sulfonic acid groups on the molecules. Thus, *sample-Cl* adsorbed 100% of the dyes present in solution, without differentiating between one dye and the other, whereas *sample-S* and *sample-Na* adsorbed between 73 and 79% of AB80 and 66% of AO7. The nonactivated waste adsorbed 47% of AO7 and 52% of AB80. These experimental results indicate that the acid sites on the surface of the adsorbents appear to favor the interaction with acid dyes. In this context and also considering the phases identified by XRD (see Figure 2), alumina and calcium aluminate are the two phases that may be more easily protonated at low pH. Although the presence of sulfate on the surface (see Figure 3, EDX analysis) increases the acidity of the solid, it also reduces the adsorption capacity of the material by interaction/repulsion with the dye molecules. The adsorption capacity remains at the same level for the sample activated with NaOH. The maximum amount of dye adsorbed at equilibrium was reached after 120 min for all samples.

The reusability of the materials was estimated from the solids separated from the liquid by centrifugation. The samples were treated with 0.1 mol/dm^3 of NaCl for 1 h to desorb the organic molecules. The saline solution was filtered from the solid by a new cycle of centrifugation, and the solid was washed several times with deionized water before being reused as the adsorbent. The process was duplicated, and the amount of AB80 and AO7 adsorbed for each reuse stage is given in Figure 5.

The comparative evolution of the amounts of dyes adsorbed with time for the single and binary solutions is shown in Figure 6. When the adsorption of the dyes occurs individually, AO7 is adsorbed to a greater extent compared to AB80. A comparison of the results obtained when the binary system is used shows clear differences between the adsorbents. Thus, *sample* and *sample-Na* adsorb high quantities of AO7, even higher than the amounts of this dye adsorbed in the single systems. This result suggests that the adsorption of AO7 is affected by the presence of AB80 during the competitive process. The increase in the adsorption of AO7 suggests that synergistic AB80 adsorption forces AO7 to be retained at sorption sites with greater affinity. *Sample-Cl* adsorbs the same amount of dyes in the binary solution as when the dyes are in single solutions. *Sample-S* adsorbs lower amount for both dye molecules. Thus, when the two molecules are adsorbed individually, the materials do not selectively adsorb either of them, only with differences in the adsorption rate at the initial stages. When both molecules are present in the same solution, *sample* and *sample-Na* selectively adsorb AO7, which may allow this molecule to be separated from AB80. Acid-activated solids exhibit practically no differences in adsorption when both molecules are present in solution, mainly in the case of *sample-Cl*.

Equations 6 and 7 were used to predict the mechanism involved in the adsorption process of dyes on activated *samples*, with the adsorption kinetic parameters being estimated by nonlinear regression (see Figure 4 and Tables S2 and S3, Supporting Information). By analyzing the coefficient of determination (R) and the chi-square test (χ^2) values of the kinetic models, the pseudo-second-order kinetic model was the best in describing the adsorption kinetics of dyes in single and binary component systems. As described in the Theoretical Approach section, such kinetic models are better considered as simple empirical equations useful for predicting the kinetics of

DOI: 10.1021/acsomega.8b02397
ACS Omega 2018, 3, 18275−18284

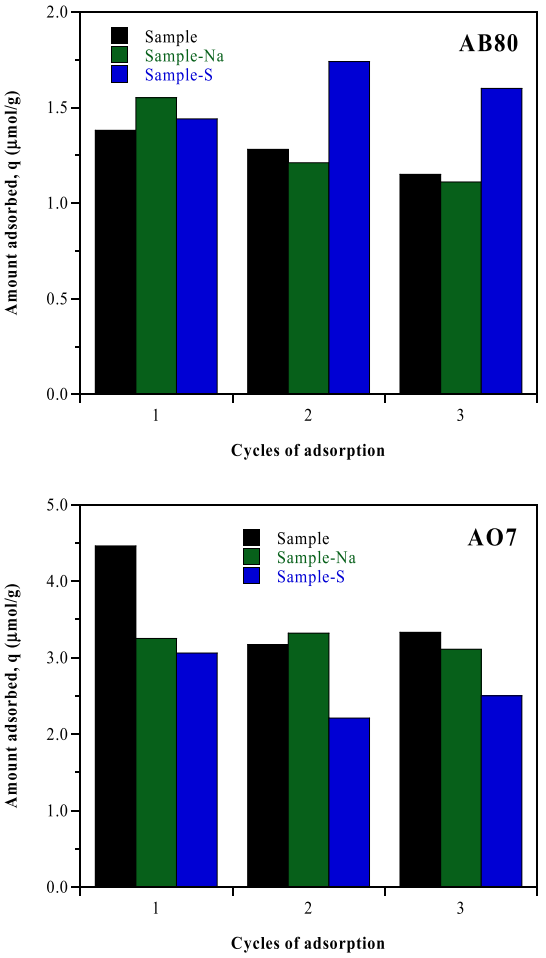

Figure 5. Reusability of the samples for AB80 and AO7 adsorption.

adsorption systems and for designing adsorption units but do not reflect the chemical and physical phenomena occurring. Additionally, as the concentrations of dyes used for this type of tests are small, adsorption in monolayer or adsorption in specific adsorption sites will be favored, which could be considered as chemisorption. In the same way, the values and trends of the constants of these models (k_1 and k_2) do not allow to reach any conclusion.

To better understand the adsorption mechanism of AO7 and AB80 on activated samples, the intraparticle diffusion model was considered. The q_t versus $t^{0.5}$ plots for the adsorption of dyes are given in Figure S1, whereas Tables S2 and S3 list the related parameters. The first linear portions represent the external mass transfer and the binding of the dye by the active sites distributed on the surface of activated samples. The second linear portions, which determine the adsorption rate, describe intraparticle diffusion and binding of dyes by active sites inside the pores of activated samples. As can be deduced from the data in Tables S2 and S3, the k_3 values increase with chemical activation, indicating fast adsorption of the dyes on the surface of the solids. Table 2 summarizes the effective diffusion coefficients. The low values of D/r^2 can be related to the limited participation of intraparticle diffusion in dye adsorption on the saline slags, also related to the low textural properties of the materials. The activation of the materials increases the diffusion coefficients, being higher for AB80 than for AO7, probably due to the sulphonic acid groups of the dye molecules (see Table S1, Supporting Information).

The equilibrium adsorption isotherm was considered important to describe the interactive behavior between adsorbates and adsorbents. Langmuir isotherm equation was thus used for modeling the experimental data. The parameters for the isotherm equation, estimated by nonlinear regression, are summarized in Table S4 (Supporting Information). The

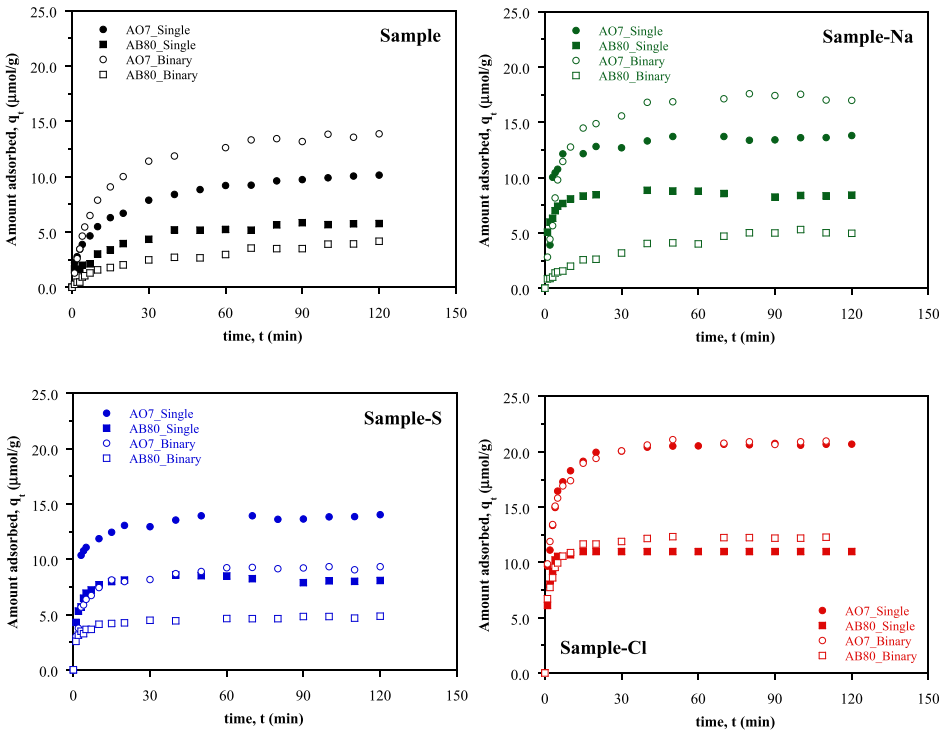

Figure 6. Kinetic adsorption data of AB80 and AO7 using samples as adsorbents for single and binary systems.

DOI: 10.1021/acsomega.8b02397
ACS Omega 2018, 3, 18275−18284

Table 2. Effective Diffusion Coefficients for AB80 and AO7 Adsorption by the Samples Indicated[a]

	sample	sample-Na	sample-S	sample-Cl
		AB80—Single		
D/r^2 (1/s)	5.3×10^{-5}	57×10^{-5}	47×10^{-5}	69×10^{-5}
χ^2	0.028	0.021	0.021	0.0030
R	0.992	0.990	0.991	0.998
		AB80—Binary		
D/r^2 (1/s)	2.7×10^{-5}	3.5×10^{-5}	33×10^{-5}	40×10^{-5}
χ^2	0.057	0.050	0.076	0.018
R	0.98	0.98	0.96	0.992
		AO7—Single		
D/r^2 (1/s)	6.3×10^{-5}	29×10^{-5}	38×10^{-5}	31×10^{-5}
χ^2	0.010	0.094	0.022	0.0084
R	0.997	0.96	0.98	0.997
		AO7—Binary		
D/r^2 (1/s)	5.8×10^{-5}	11×10^{-5}	19×10^{-5}	29×10^{-5}
χ^2	0.022	0.036	0.032	0.020
R	0.995	0.990	0.98	0.991

[a] T = 25 °C, C_0 = 15 mg/dm^3 (0.022 mmol/dm^3 for AB80 and 0.022 mmol/dm^3 for AO7), and pH = 2.

affinity parameters of the adsorbents, k_L, confirm the results obtained under kinetic conditions. From them, it was observed that AO7 had more affinity for the materials than AB80. In the case of the binary mixtures, the values of the coefficients change slightly.

2.3. CO_2 Adsorption Experiments. The CO_2 adsorption capacity of the samples at three temperatures and pressures up to 80 kPa are shown in Figure 7. The adsorbed CO_2 evolution with the temperature indicates that there is a physical interaction between the surface of the solids and CO_2. The aluminum saline slag, *sample*, showed higher adsorption capacity than the wastes. At low pressures, *sample* and *sample-Na* show a similar and high capacity of adsorption, but at high pressures, the differences are more important. The adsorption at low pressures can be related to the interaction with specific sites of adsorption, estimated in this case by pHpzc and V(NH_3), see Table 1. The differences in textural properties can explain the results at high pressures.[44] *Sample* shows a specific surface area of 84 m^2/g and a micropore volume of 0.010 cm^3/g in comparison to 42 m^2/g and 0.002 cm^3/g shown by *sample-Na*. In the case of the samples treated with acids, the low adsorption capacity of CO_2 at low pressures with respect to the results observed for *sample* and *sample-Na* can be explained by the differences between pHpzc and V(NH_3), from 2.0−3.7 to 8.6−9.7 for pHpzc and from 5.21−5.22 to 2.84−3.35 cm^3/g for V(NH_3). The low textural properties of the samples treated with acids also explain the results at high pressures. The experimental results indicate that the aluminum saline slags can be used as adsorbents to retain CO_2 and that the chemical activation of these solids does not increase their adsorption capacity.

A comparison of the Henry's constants (H), obtained from the isotherms in the low-pressure region (Table 3), showed that the constants were higher for *sample* and *sample-Na* than for *sample-S* and *sample-Cl*, and that the values decreased as the temperature increased. This behavior is related to a more important interaction of CO_2 on the surface of the wastes at low temperatures and pressures. These results are also used to calculate the limiting heat, q_{st}^0, by applying the Clausius−Clapeyron equation in the low-pressure region.[45] The isosteric heats obtained are included in Table 3, showing that the values

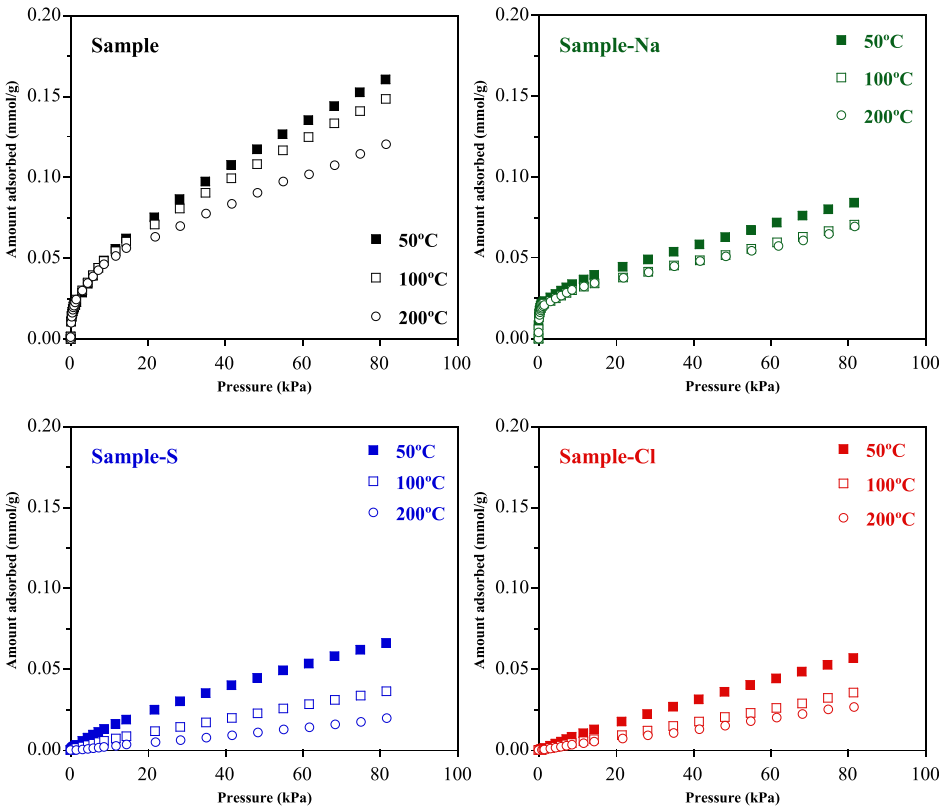

Figure 7. CO_2 adsorption on the samples at 50, 100, and 200 °C.

DOI: 10.1021/acsomega.8b02397
ACS Omega 2018, 3, 18275−18284

Table 3. Henry's Constants for CO_2 Adsorption at Several Temperatures and Isosteric Heats of Adsorption at Zero Coverage by the Samples Indicated

samples/temperature (°C)	H (mmol/kPa·g)	q_{st}^0 (kJ/mol)[a]
Sample		
50	55.4×10^{-3}	
100	58.5×10^{-3}	1.7
200	52.8×10^{-3}	
Sample-Na		
50	71.4×10^{-3}	
100	65.7×10^{-3}	1.7
200	58.6×10^{-3}	
Sample-S		
50	3.0×10^{-3}	
100	0.75×10^{-3}	26.8
200	0.13×10^{-3}	
Sample-Cl		
50	0.48×10^{-3}	
100	0.22×10^{-3}	9.6
200	0.15×10^{-3}	

[a]From the Henry constant.

for *sample* and *sample-Na* were lower than for *sample-S* and *sample-Cl* in accordance with the adsorption capacity in this range of pressures.

The dependence of the isosteric heats of adsorption, calculated using the Clausius−Clapeyron equation, on the amount adsorbed for the samples is shown in Figure 8. The

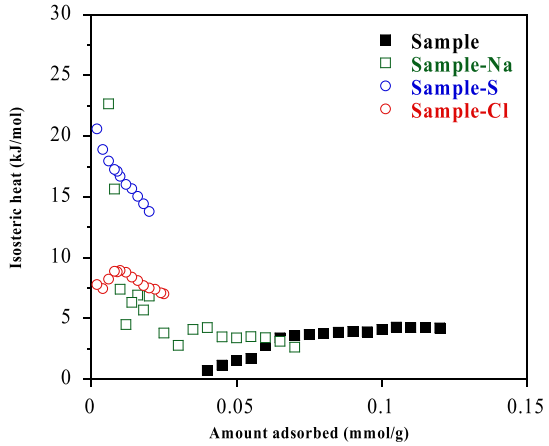

Figure 8. Isosteric heat of CO_2 adsorption as a function of the amount of CO_2 adsorbed on the samples.

results obtained show that for *sample* and *sample-Cl*, the isosteric heats are constant with loading, increasing at low loading in the case of *sample-Na* and *sample-S*. Schwaab et al.[46] reported that the evolution of the isosteric heats with adsorbate loading can be related to the energetically homogeneous/heterogeneous character of the adsorbents. In the case of *sample* and *sample-Cl*, the samples are energetically homogeneous toward CO_2 adsorption. In the same way, *sample* and *sample-S* are energetically heterogeneous.

3. SUMMARY AND CONCLUSIONS

Herein, we have presented wastes produced, after the extraction of aluminum from saline slags generated during secondary aluminum recycling processes, as adsorbents for organic contaminants in contaminated liquid streams and CO_2 removal. The materials were obtained by the treatment of saline slags with 2 mol/dm^3 aqueous solutions of NaOH, H_2SO_4, and HCl under reflux conditions, which at the same time extracts a valuable amount of aluminum from the slag. The treatments modify the acidity−basicity properties of the solids. The resulting materials have been used as adsorbents for the removal of the acid dyes Acid Orange 7 and Acid Blue 80, considering single and binary component systems, and CO_2 storage.

Taking into account the individual solutions, the preferential adsorption of AB80 compared to AO7 seems to be related to the number of sulfonic acid groups present in the dye molecules. The treatment of saline slag with aqueous solutions of HCl increases the acidic properties of the solids and their dye-adsorption capacity. In the case of treatment with aqueous H_2SO_4 solutions, the adsorption capacity of dyes is not favored by the presence of sulfate groups on the surface. A preferential adsorption of AO7 is observed compared to AB80 in binary solutions when using the starting material and the NaOH-treated solid. No preferential adsorption is found in the case of the adsorbents obtained upon treatment with acids. Kinetic results allow to deduce that the adsorption of AO7 and AB80 on the aluminum saline slags takes place via a monolayer adsorption process. As a final conclusion, untreated starting materials or those treated with a base could be suitable for separating the components from the binary solutions.

The evolution of the amount of CO_2 adsorbed with the temperature indicates that there is a physical interaction between the surface of the wastes and CO_2. The adsorption on specific sites and the textural properties can explain the differences between the materials. The isosteric heats of CO_2 adsorption from the Clausius−Clapeyron equation varied in the range of 1.7−26.8 kJ/mol.

4. EXPERIMENTAL PROCEDURE

4.1. Materials. Reagents used for the chemical activation of the aluminum saline slags were NaOH (Panreac), H_2SO_4 (98%, Panreac), and HCl (37%, Acros). Acid Blue 80 (Merck, 40%) and Acid Orange 7 (Aldrich, 85%) were selected as representative acid dyes. NH_3 (Air Liquide, >99.995%), CO_2 (Praxair, 99.990%), N_2 (Praxair, 99.999%), and He (Air Liquide, 99.998%) were also used.

4.2. Adsorbents from Wastes. An aluminum saline slag previously treated with hot water was used as the material. The procedure and conditions for aluminum extraction with NaOH, H_2SO_4, and HCl are reported in previous works.[4,47] The results of aluminum extracted, determined by inductively coupled plasma atomic emission spectroscopy, are included in Figure S2 (Supporting Information), and the aluminum thus extracted was used for the synthesis of new materials.[47] After the chemical reaction for aluminum extraction, the slurries were separated by filtration and washed several times with deionized water. The solids obtained, that is, the residual wastes, were dried at 60 °C for 16 h and considered as adsorbents of acid dyes and CO_2. The nomenclature used for these solids is *sample-Y*, where Y is the reagent used in the chemical activation. Thus, for example, *sample-Na* is a solid treated with an aqueous solution of 2 mol/dm^3 NaOH for 2 h under reflux conditions.

4.3. Characterization Techniques. N_2 (Praxair, 99.999%) adsorption−desorption measurements were obtained at −196 °C from a Micromeritics ASAP 2010

DOI: 10.1021/acsomega.8b02397
ACS Omega 2018, 3, 18275−18284

adsorption analyzer. The powder XRD patterns of the materials were carried out using a Siemens D-5000 diffractometer. SEM analysis of the samples was considered using a JEOL microscope, model JSM-6400.

pHpzc was determined from mass titrations by a procedure previously reported.[41]

The acidity of the samples was determined by adsorption of NH_3 using a dynamic pulse method. The procedure and conditions are reported in a previous work.[48]

4.4. CO_2 Adsorption Experiments. The procedure and conditions used for adsorption of CO_2 at several temperatures are reported in a previous work.[47]

4.5. Dye Adsorption Procedure. Acid Blue 80 (AB80) and Acid Orange 7 (AO7) were selected as anionic dyes for this research. The properties of the dyes are summarized in Table S1 (Supporting Information). The concentration of the dye molecules in aqueous solutions was determined by an ultraviolet−visible spectrophotometer, Jasco V-730, at the maxima wavelength of absorption found, 485 and 627 nm for AO7 and AB80. The maximum absorbance was confirmed by scanning aqueous solutions of the dye over the spectral range of 290−800 nm. As the absorbance peaks are well-separated in binary solutions, they can be used for concentration measurements. Calibration curves for both individual dyes and the binary system were carried out at a pH value of 2; this pH value was also used for the adsorption processes (see below).

The adsorption kinetics experiments were evaluated in the batch mode. Thus, three stock solutions of Acid Orange 7 (15 mg/dm^3, 0.022 mmol/dm^3), Acid Blue 80 (15 mg/dm^3, 0.043 mmol/dm^3), and a binary system containing AO7 and AB80 (ratio of 1:1, totalizing 30 mg/dm^3) were used. In a typical experiment, 0.2 g of the adsorbent was placed in contact with 100 cm^3 of the dye solution at a pH value of 2, and the mixture was stirred for predetermined intervals of time (between 0.5 and 120 min). The solution was then separated from the adsorbent by filtration using Durapore membrane filters with a pore size of 0.45 μm. The amount of dye adsorbed on the waste (q_t) was calculated by the equation

$$q_{t,e} = V\cdot(C_0 - C_{t,e})/m \tag{1}$$

where C_0 is the initial concentration (μmol/dm^3), C_t is the concentration (μmol/dm^3) at a certain adsorption time t (min), V is the solution volume (dm^3), and m is the amount of sample added (g).

The equilibrium adsorption capacity was determined from various initial concentrations of the dyes. The procedure and conditions are reported in a previous work.[49] The amount of dye adsorbed on the material at equilibrium (q_e) was determined according to eq 1, where C_e (μmol/dm^3) is the concentration of the dye at equilibrium. All experiments were carried out in duplicate.

4.4.1. Theoretical Approach: Adsorption Kinetics. The transport of adsorbate molecules inside porous adsorbents can be described by two types of kinetic modeling approaches.[50] The first type of model considers simple relationships between the adsorption process and the operating conditions. These types of models describe how the average solid-phase concentration (q) changes with the time of adsorption. Pseudo-first- and pseudo-second-order rate equations are included in this category. The second approach includes phenomenological models that attempt to describe the adsorption rate through the resistances of external mass transfer, intraparticle diffusion, and adsorption on the sites. Information on the adsorption mechanism can be obtained from the second type of models using the kinetic experimental results and the equilibrium adsorption data.

Considering mass balances to the liquid phase in the batch system and assuming first- and second-order kinetics for the driving force term, the following equations are obtained

$$-\frac{dn}{dt} = -V\frac{dC}{dt} = k_1\cdot V\cdot(C - C_e) \tag{2}$$

$$-\frac{dn}{dt} = -V\frac{dC}{dt} = k_2\cdot\frac{V^2}{m}\cdot(C - C_e)^2 \tag{3}$$

where n (mmol) is the amount of organic molecule in the liquid phase, V (cm^3) is the volume of the solution, C (mmol/dm^3) is the organic molecule concentration in the solution, m (g) is the adsorbent mass, t (min) is the contact time, and k_1 (1/min) and k_2 (g/mmol·min) are the adsorption kinetic constants of the pseudo-first- and pseudo-second-order.

The equations can be integrated between the initial time and time t and by considering the initial conditions (for $t = 0$, $C = C_0$). Under these situations, the following equations are obtained

$$\ln\left(\frac{C_t - C_e}{C_0 - C_e}\right) = -k_1\cdot t \tag{4}$$

$$C_t = C_e + \frac{V\cdot m\cdot(C_0 - C_e)}{m + k_2\cdot V\cdot(C_0 - C_e)\cdot t} \tag{5}$$

The equations can also be expressed considering the relationship between the organic molecule concentration in the aqueous solution (C) and in the solid phase (q) as

$$q_t = q_e\cdot(1 - \exp(-k_1\cdot t)) \tag{6}$$

$$q_t = \frac{k_2\cdot q_e^{\,2}\cdot t}{1 + k_2\cdot q_e\cdot t} \tag{7}$$

These two equations have been employed to explain the adsorption of aqueous pollutants on adsorbents.[4,51−56]

The intraparticle diffusion model is applicable only within restrictive conditions. This model assumes that intraparticle diffusion is the rate-controlling step of the adsorption process.[57] This is the case when well-mixed solutions are considered. Under these situations, the intraparticle diffusivity is constant, and the uptake of the adsorbate by the material is small if the total quantity of the adsorbate present in the solution is taken into consideration. The equation for this model is

$$q_t = k_3\cdot t^{0.5} \tag{8}$$

where k_3 (mmol/g·min$^{0.5}$) is the intraparticle diffusion rate constant. This model has been previously applied to several adsorption systems.[9,51,54,58,59]

The effective diffusion coefficient can be calculated from the fractional approach to the equilibrium, $F(t)$[60]

$$F(t) = \frac{C_0 - C_t}{C_0 - C_e} = \left[1 - \exp\left(-\frac{\pi^2\cdot D\cdot t}{r^2}\right)\right]^{0.5} \tag{9}$$

where D (m^2/s) is the intraparticle diffusion coefficient and r (m) is the particle size radius assuming a spherical geometry.

DOI: 10.1021/acsomega.8b02397
ACS Omega 2018, 3, 18275−18284

4.4.2. Theoretical Approach: Equilibrium. The adsorption equilibrium is often expressed by various isotherm equations.[50] The Langmuir model considers monolayer coverage of adsorbent surfaces and can be represented for multicomponent studies as

$$q_{e,i} = \frac{k_{L,i} \cdot q_{L,i} \cdot C_{e,i}}{1 + \sum_{j=1}^{N} k_{L,j} \cdot C_{e,j}} \quad (10)$$

where $k_{L,i}$ ($dm^3/\mu mol$) and $q_{L,i}$ ($\mu mol/g$) are Langmuir constants that represent the equilibrium adsorption related to the affinity of binding sites and the monolayer adsorption capacity. This equation assumes that all adsorbates compete for energetically identical adsorption sites.

■ ASSOCIATED CONTENT

Supporting Information

The Supporting Information is available free of charge on the ACS Publications website at DOI: 10.1021/acsomega.8b02397.

Characteristics of the dyes studied as adsorbates, kinetics parameters for dye adsorption, and aluminum extracted under several conditions (PDF)

■ AUTHOR INFORMATION

Corresponding Author

*E-mail: andoni@unavarra.es. Phone: +34 948 169602 (A.G.).

ORCID

Antonio Gil: 0000-0001-9323-5981

Miguel Ángel Vicente: 0000-0002-6714-0249

Notes

The authors declare no competing financial interest.

■ ACKNOWLEDGMENTS

The authors are grateful for the financial support from the Seventh Framework Programme through the project RecycAl, the Spanish Ministry of Economy, Industry, and Competitiveness (*AEI/MINECO*), and the European Regional Development Fund (ERDF) through project MAT2016-78863-C2-R. A.G. also thanks Santander Bank for funding through the Research Intensification Program.

■ REFERENCES

(1) Reife, A.; Freeman, H. S. *Environmental Chemistry of Dyes and Pigments*; John Wiley & Sons: New York, 1996.

(2) Eckenfelder, W. W., Jr. Wastewater Treatment. *Kirk-Othmer: Chemical Technology and the Environment*; John Wiley & Sons: New York, 2007; pp 577−614.

(3) Yagub, M. T.; Sen, T. K.; Afroze, S.; Ang, H. M. Dye and its removal from aqueous solution by adsorption: A review. *Adv. Colloid Interface Sci.* **2014**, *209*, 172−184.

(4) Gil, A.; Albeniz, S.; Korili, S. A. Valorization of the saline slags generated during secondary aluminium melting processes as adsorbents for the removal of heavy metal ions from aqueous solutions. *Chem. Eng. J.* **2014**, *251*, 43−50.

(5) McKay, G.; Al-Duri, B. Extended empirical Freundlich isotherm for binary systems: a modified proce dure to obtain the correlative constants. *Chem. Eng. Process.* **1991**, *29*, 133−138.

(6) Choy, K. K. H.; Porter, J. F.; McKay, G. Langmuir Isotherm Models Applied to the Multicomponent Sorption of Acid Dyes from Effluent onto Activated Carbon. *J. Chem. Eng. Data* **2000**, *45*, 575−584.

(7) Rio, S.; Delebarre, A.; Héquet, V.; Le Cloirec, P.; Blondin, J. Metallic ion removal from aqueous solutions by fly ashes: multicomponent studies. *J. Chem. Technol. Biotechnol.* **2002**, *77*, 382−388.

(8) Choy, K. K. H.; Porter, J. F.; McKay, G. Single and multicomponent equilibrium studies for the adsorption of acidic dyes on carbon from effluents. *Langmuir* **2004**, *20*, 9646−9656.

(9) Choy, K. K. H.; Porter, J. F.; Mckay, G. Intraparticle diffusion in single and multicomponent acid dye adsorption from wastewater onto carbon. *Chem. Eng. J.* **2004**, *103*, 133−145.

(10) Choy, K. K. H.; Allen, S. J.; Mckay, G. Multicomponent equilibrium studies for the adsorption of basic dyes from solution on lignite. *Adsorption* **2005**, *11*, 255−259.

(11) Chiou, M.-S.; Chuang, G.-S. Competitive adsorption of dye metanil yellow and RB15 in acid solutions on chemically cross-linked chitosan beads. *Chemosphere* **2006**, *62*, 731−740.

(12) Al-Degs, Y.; Khraisheh, M. A. M.; Allen, S. J.; Ahmad, M. N.; Walker, G. M. Competitive adsorption of reactive dyes from solution: equilibrium isotherm studies in single and multisolute systems. *Chem. Eng. J.* **2007**, *128*, 163−167.

(13) Turabik, M. Adsorption of basic dyes from single and binary component systems onto bentonite: simultaneous analysis of basic red 46 and basic yellow 28 by first order derivative spectrophotometric analysis method. *J. Hazard. Mater.* **2008**, *158*, 52−64.

(14) Noroozi, B.; Sorial, G. A.; Bahrami, H.; Arami, M. Adsorption of binary mixtures of cationic dyes. *Dyes Pigm.* **2008**, *76*, 784−791.

(15) Chan, L. S.; Cheung, W. H.; Allen, S. J.; McKay, G. Separation of acid-dyes mixture by bamboo derived active carbon. *Sep. Purif. Technol.* **2009**, *67*, 166−172.

(16) Pura, S.; Atun, G. Adsorptive Removal of Acid Blue 113 and Tartrazine by Fly Ash from Single and Binary Dye Solutions. *Sep. Sci. Technol.* **2009**, *44*, 75−101.

(17) Atun, G.; Acar, E. T. Competitive adsorption of basic dyes onto calcite in single and binary component systems. *Sep. Sci. Technol.* **2010**, *45*, 1471−1481.

(18) Mahmoodi, N. M.; Salehi, R.; Arami, M. Binary system dye removal from colored textile wastewater using activated carbon: kinetic and isotherm studies. *Desalination* **2011**, *272*, 187−195.

(19) Fernandez, M. E.; Bonelli, P. R.; Cukierman, A. L.; Lemcoff, N. O. Modeling the biosorption of basic dyes from binary mixtures. *Adsorption* **2015**, *21*, 177−183.

(20) Duta, A.; Visa, M. Simultaneous removal of two industrial dyes by adsorption and photocatalysis on a fly-ash-TiO2 composite. *J. Photochem. Photobiol., A* **2015**, *306*, 21−30.

(21) Yu, J.-x.; Zhu, J.; Feng, L.-y.; Chi, R.-a. Simultaneous removal of cationic and anionic dyes by the mixed sorbent of magnetic and non-magnetic modified sugarcane bagasse. *J. Colloid Interface Sci.* **2015**, *451*, 153−160.

(22) Mazaheri, H.; Ghaedi, M.; Asfaram, A.; Hajati, S. Performance of CuS nanoparticle loaded on activated carbon in the adsorption of methylene blue and bromophenol blue dyes in binary aqueous solutions: Using ultrasound power and optimization by central composite design. *J. Mol. Liq.* **2016**, *219*, 667−676.

(23) Yang, L.; Zhang, Y.; Liu, X.; Jiang, X.; Zhang, Z.; Zhang, T.; Zhang, L. The investigation of synergistic and competitive interaction between dye Congo red and methyl blue on magnetic MnFe2O4. *Chem. Eng. J.* **2014**, *246*, 88−96.

(24) Mahmoodi, N. M.; Hosseinabadi-Farahani, Z.; Chamani, H. Dye adsorption from single and binary systems using NiO-MnO2nanocomposite and artificial neural network modeling. *AIChE J.* **2016**, *36*, 111−119.

(25) Stawiński, W.; Węgrzyn, A.; Dańko, T.; Freitas, O.; Figueiredo, S.; Chmielarz, L. Acid-base treated vermiculite as high performance adsorbent: Insights into the mechanism of cationic dyes adsorption, regeneration, recyclability and stability studies. *Chemosphere* **2017**, *173*, 107−115.

(26) Choi, S.; Drese, J. H.; Jones, C. W. Adsorbent materials for carbon dioxide capture from large anthropogenic point sources. *ChemSusChem* **2009**, *2*, 796−854.

DOI: 10.1021/acsomega.8b02397
ACS Omega 2018, 3, 18275−18284

(27) Wang, J.; Huang, L.; Yang, R.; Zhang, Z.; Wu, J.; Gao, Y.; Wang, Q.; O'Hare, D.; Zhong, Z. Recent advances in solid sorbents for CO2 capture and new development trends. *Energy Environ. Sci.* **2014**, *7*, 3478−3518.
(28) Garcés, S. I.; Villarroel-Rocha, J.; Sapag, K.; Korili, S. A.; Gil, A. Comparative Study of the Adsorption Equilibrium of CO2 on Microporous Commercial Materials at Low Pressures. *Ind. Eng. Chem. Res.* **2013**, *52*, 6785−6793.
(29) Garcés-Polo, S. I.; Villarroel-Rocha, J.; Sapag, K.; Korili, S. A.; Gil, A. Adsorption of CO2 on mixed oxides derived from hydrotalcites at several temperatures and high pressures. *Chem. Eng. J.* **2018**, *332*, 24−32.
(30) D'Alessandro, D. M.; Smit, B.; Long, J. R. Carbon dioxide capture: prospects for new materials. *Angew. Chem., Int. Ed.* **2010**, *49*, 6058−6082.
(31) Olivares-Marín, M.; Maroto-Valer, M. M. Development of adsorbents for CO2 capture from waste materials: a review. *Greenhouse Gases: Sci. Technol.* **2012**, *2*, 20−35.
(32) Ives, M.; Mundy, R. C.; Fennell, P. S.; Davidson, J. F.; Dennis, J. S.; Hayhurst, A. N. Comparison of Different Natural Sorbents for Removing CO2from Combustion Gases, as Studied in a Bench-Scale Fluidized Bed. *Energy Fuels* **2008**, *22*, 3852−3857.
(33) Li, Y.; Liu, C.; Sun, R.; Liu, H.; Wu, S.; Lu, C. Sequential SO2/CO2 Capture of Calcium-Based Solid Waste from the Paper Industry in the Calcium Looping Process. *Ind. Eng. Chem. Res.* **2012**, *51*, 16042−16048.
(34) Olivares-Marín, M.; Drage, T. C.; Maroto-Valer, M. M. Novel lithium-based sorbents from fly ashes for CO2 capture at high temperatures. *Int. J. Greenhouse Gas Control* **2010**, *4*, 623−629.
(35) Gil, A.; Arrieta, E.; Vicente, M. A.; Korili, S. A. Synthesis and CO2 adsorption properties of hydrotalcite-like compounds prepared from aluminum saline slag wastes. *Chem. Eng. J.* **2018**, *334*, 1341−1350.
(36) Ip, A. W. M.; Barford, J. P.; McKay, G. Reactive black dye adsorption/desorption onto different adsorbents: Effect of salt, surface chemistry, pore size and surface area. *J. Colloid Interface Sci.* **2009**, *337*, 32−38.
(37) Aznárez, A.; Gil, A.; Korili, S. A. Performance of palladium and platinum supported on alumina pillared clays in the catalytic combustion of propene. *RSC Adv.* **2015**, *5*, 82296−82309.
(38) Gil, A.; Santamaría, L.; Korili, S. A. Removal of caffeine and diclofenac from aqueous solution by adsorption on multiwalled carbon nanotubes. *Colloid Interface Sci. Commun.* **2018**, *22*, 25−28.
(39) Do, D. D. *Adsorption Analysis: Equilibria and Kinetics*; Imperial College Press: London, 1998.
(40) Gil, A.; Assis, F. C. C.; Albeniz, S.; Korili, S. A. Removal of dyes from wastewaters by adsorption on pillared clays. *Chem. Eng. J.* **2011**, *168*, 1032−1040.
(41) Hasan, Z.; Jeon, J.; Jhung, S. H. Adsorptive removal of naproxen and clofibric acid from water using metal-organic frameworks. *J. Hazard. Mater.* **2012**, *209−210*, 151−157.
(42) Kyzas, G. Z.; Kostoglou, M.; Lazaridis, N. K.; Lambropoulou, D. A.; Bikiaris, D. N. Environmental friendly technology for the removal of pharmaceutical contaminants from wastewaters using modified chitosan adsorbents. *Chem. Eng. J.* **2013**, *222*, 248−258.
(43) Álvarez-Torrellas, S.; Rodríguez, A.; Ovejero, G.; García, J. Comparative adsorption performance of ibuprofen and tetracycline from aqueous solution by carbonaceous materials. *Chem. Eng. J.* **2016**, *283*, 936−947.
(44) Essandoh, M.; Kunwar, B.; Pittman, C.U., Jr.; Mohan, D.; Mlsna, T. Sorptive removal of salicylic acid and ibuprofen from aqueous solutions using pine wood fast pyrolysis biochar. *Chem. Eng. J.* **2015**, *265*, 219−227.
(45) Gil, A.; Taoufik, N.; García, A. M.; Korili, S. A. Comparative removal of emerging contaminants from aqueous solution by adsorption on an activated carbon. *Environ. Technol.* **2018** (in press). DOI: 10.1080/09593330.2018.1464066
(46) Schwaab, M.; Steffani, E.; Barbosa-Coutinho, E.; Severo Júnior, J. B. Critical analysis of adsorption/diffusion modelling as a function of time square root. *Chem. Eng. Sci.* **2017**, *173*, 179−186.
(47) El Qada, E. N.; Allen, S. J.; Walker, G. M. Kinetic modeling of the adsorption of basic dyes onto steam-activated bituminous coal. *Ind. Eng. Chem. Res.* **2007**, *46*, 4764−4771.
(48) Sze, M. F. F.; McKay, G. An adsorption diffusion model for removal of para-chlorophenol by activated carbon derived from bituminous coal. *Environ. Pollut.* **2010**, *158*, 1669−1674.
(49) Khraisheh, M. A. M.; Al-Degs, Y. S.; Allen, S. J.; Ahmad, M. N. Elucidation of controlling steps of reactive dye adsorption on activated carbon. *Ind. Eng. Chem. Res.* **2002**, *41*, 1651−1657.
(50) Gregg, S. J.; Sing, K. S. W. *Adsorption, Surface Area and Porosity*; Academic Press: New York, 1991.
(51) Rouquerol, J.; Avnir, D.; Fairbridge, C. W.; Everett, D. H.; Haynes, J. M.; Pernicone, N.; Ramsay, J. D. F.; Sing, K. S. W.; Unger, K. K. Recommendations for the characterization of porous solids. *Pure Appl. Chem.* **1994**, *66*, 1739−1758.
(52) Gil, A.; Korili, S. A. Management and valorization of aluminum saline slags: Current status and future trends. *Chem. Eng. J.* **2016**, *289*, 74−84.
(53) Yoshimura, H. N.; Abreu, A. P.; Molisani, A. L.; de Camargo, A. C.; Portela, J. C. S.; Narita, N. E. Evaluation of aluminum dross waste as raw material for refractories. *Ceram. Int.* **2008**, *34*, 581−591.
(54) Huang, X.-L.; El Badawy, A. M.; Arambewela, M.; Adkins, R.; Tolaymat, T. Mineral phases and metals in baghouse dust from secondary aluminum production. *Chemosphere* **2015**, *134*, 25−30.
(55) Tsakiridis, P. E.; Oustadakis, P.; Moustakas, K.; Agatzini, S. L. Cyclones and fabric filters dusts from secondary aluminium flue gases: a characterization and leaching study. *Int. J. Environ. Sci. Technol.* **2016**, *13*, 1793−1802.
(56) Hamoud, H. I.; Finqueneisel, G.; Azambre, B. Removal of binary dyes mixtures with opposite and similar charges by adsorption, coagulation/flocculation and catalytic oxidation in the presence of CeO_2/H_2O_2 Fenton-like system. *J. Environ. Manage.* **2017**, *195*, 195−207.
(57) Duta, A.; Visa, M. Simultaneous removal of two industrial dyes by adsorption and photocatalysis on a fly-ash-TiO_2 composite. *J. Photochem. Photobiol., A* **2015**, *306*, 21−30.
(58) Wang, K.; Qiao, S.; Hu, X. Study of isosteric heat of adsorption and activation energy for surface diffusion of gases on activated carbon using equilibrium and kinetics information. *Sep. Purif. Technol.* **2004**, *34*, 165−176.
(59) Sircar, S. Excess properties and thermodynamics of multicomponent gas adsorption. *J. Chem. Soc., Faraday Trans. 1* **1985**, *81*, 1527−1540.
(60) Sircar, S.; Mohr, R.; Ristic, C.; Rao, M. B. Isosteric heat of adsorption: theory and experiment. *J. Phys. Chem. B* **1999**, *103*, 6539−6546.

DOI: 10.1021/acsomega.8b02397
ACS Omega 2018, 3, 18275−18284